coatings

MDPI

Article

Rust Conversion Performance of Phosphoric Acid-Gallic Acid in Vinyl Chloride Acrylic Emulsion

Xin Wang [1,2,3,4], Qingjun Zhu [1,2,3,4,*], Xiangju Liu [1,3,4] and Baorong Hou [1,2,3,4,*]

1 CAS Key Laboratory of Marine Environmental Corrosion and Bio-Fouling, Institute of Oceanology, Chinese Academy of Sciences, Qingdao 266071, China; wangxin183@mails.ucas.ac.cn (X.W.); liuxiangju124@163.com (X.L.)
2 College of Earth and Planetary Sciences, University of Chinese Academy of Sciences, Beijing 100049, China
3 Open Studio for Marine Corrosion and Protection, Pilot National Laboratory for Marine Science and Technology (Qingdao), Qingdao 266237, China
4 Center for Ocean Mega-Science, Chinese Academy of Sciences, 7 Nanhai Road, Qingdao 266071, China
* Correspondence: zhuqingjun@qdio.ac.cn (Q.Z.); baoronghou@163.com (B.H.)

Abstract: This work studied the application of phosphoric acid-gallic acid in vinyl chloride acrylic emulsion and its rust conversion performance. The increase of phosphoric acid affected the stability of the system, leading to the rapid precipitation of flocculent precipitation. Rust conversion coating (RCC) showed the best synergistic conversion effect when gallic acid (GA) was 0.2 wt.% and phosphoric acid (PA) was 2 wt.%. XRD and FTIR analysis show that the components of adherent rust (AR) are α-FeOOH, γ-FeOOH and Fe_3O_4. The conversion products are ferric phosphate (FP) and ferric gallate (FG). The RCC can effectively treat the rusted steel (RS) produced by simulated marine atmospheric corrosion. The corrosion current density was reduced by three orders of magnitude, the adhesion reached 2.75 MPa, and the salt spray corrosion resistance was 20 days. The results of Raman, XPS, SEM and EDS show that the ionic dissolution of iron, complexation and further oxidation reactions occur at the interface between the adherent rust and the RCC. After rust conversion treatment, unreacted rust (UR) affects the further improvement of adhesion strength and anti-corrosion performance.

Keywords: rust conversion coating; anticorrosion; gallic acid; acrylic emulsion; rust converter

Citation: Wang, X.; Zhu, Q.; Liu, X.; Hou, B. Rust Conversion Performance of Phosphoric Acid-Gallic Acid in Vinyl Chloride Acrylic Emulsion. *Coatings* **2021**, *11*, 152. https://doi.org/10.3390/coatings11020152

Academic Editor: Pier Luigi Bonora
Received: 15 January 2021
Accepted: 27 January 2021
Published: 29 January 2021

1. Introduction

The cost of metal corrosion is huge [1–5], and it always threatens the safety of human life. In recent years, a large number of steel structures need to be maintained in various countries around the world. Many corroded parts are not easy to replace and need to be repainted on the original substrate. In order to ensure that the recoated coating has good adhesion and anti-corrosion properties, it is necessary to use sand blasting, shot blasting and other methods to remove the rust on the substrate. The cost of the above method is very high, and it will also cause dust and noise pollution. At the same time, some complex structures are difficult to remove rust manually. Therefore, rust conversion coating (RCC) has attracted the attention of researchers. RCC can be used on steel that has not been sufficiently derusted (≥St2, ISO 8501-1: 2007 [6]). It converts rust into harmless inert compounds, thereby preventing corrosion.

Reasonable application of RCC must pay attention to the nature and interaction of rust (composition [7–10] and structure [11]) and rust converter (type [12], conversion capacity [13] and concentration [14]). Before using the RCC, the nonadherent rust (NAR) on the surface of the rusted steel needs to be removed [15]. Vegetable tannin has been used as rust converter because they contain a large amount of hydroxyl groups. Hydroxyl groups can react with iron ions to form blue-violet complex [16,17]. Tannic acid and gallic acid are both regarded as model compounds of tannin. Previous research mainly focused

on the corrosion inhibition [14,18] and rust conversion performance [19–21] of tannic acid, phosphoric acid or their mixtures. However, rust converters and RCC based on gallic acid are rarely studied. Favre et al. [22] revealed the anti-corrosion mechanism of gallic acid and believed that gallic acid inhibited the process of reducing γ-FeOOH to Fe_3O_4. Liu et al. [23] prepared a rust conversion emulsion with gallic acid, which has good adhesion and corrosion resistance.

With the improvement of human environmental protection awareness, water-based coatings have developed rapidly due to low volatile organic compounds (VOC). Adding rust converter to water-based resin to prepare water-based RCC has become popular [24]. Vinyl chloride acrylic emulsion is suitable for RCC [25], because it will not demulsify due to the addition of acidic rust converters. This work studied the application of phosphoric acid-gallic acid in vinyl chloride acrylic emulsion. The influence of the amount of phosphoric acid and gallic acid on the rust conversion system was explored. Tafel curve analysis, salt spray test and adhesion test are used to study the anti-corrosion performance of RCC. XRD and FTIR techniques were used to characterize the components of adherent rust and conversion products. Raman and XPS techniques were used to analyze the surface composition changes of the rusted steel substrate. In addition, the cross-sectional morphology and element distribution of the RCC were observed by SEM and EDS. The results explained the rust conversion mechanism of phosphoric acid-gallic acid in vinyl chloride acrylic emulsion.

2. Materials and Methods

2.1. Raw Materials and Sample Preparation

2.1.1. Materials

The gallic acid (analytical reagent) used in this work was a commercially reagent purchased from Shanghai Aladdin Biochemical Technology Corporation. Vinyl chloride acrylic emulsion (Haloflex 202) was obtained from DSM Corporation. Texanol with the effective chemical composition of 2,2,4-trimethyl-1,3-pentanediol monoisobutyrate was purchased from EASTMAN Company. Foamaster MO 2134AC was purchased from BASF Corporation. Phosphoric acid (analytical reagent), anhydrous ethanol (analytical reagent), sodium chloride (analytical reagent) and acetone (analytical reagent) were purchased from Sinopharm Chemical Reagent Company. Water used throughout the experiments was made by a pure-ultrapure water system that was distilled and deionized with resistance of 18.2 MΩ cm. None of the above materials were further processed.

2.1.2. Preparation of Rusted Steel

Compositions of the Q235 steel used are listed as follows (wt.%): C $\leq$ 0.19, Mn $\leq$ 0.59, Si $\leq$ 0.3, S $\leq$ 0.05, P $\leq$ 0.044, Fe (balance). The steel plates were degreased successively by ultrasonic cleaning with ethanol for 15 min and acetone for 30 min, and finally rinsed with ethanol and dried. The steel plates (thickness 2 mm) were first immersed in 3.5% NaCl for 20 min, and then stored at 35 °C and 96% relative humidity in temperature and humidity chamber until uniform rust layer is formed. After the pre-corrosion period, the steel plates were hand-cleaned by wire-brush to remove the nonadherent rust and remain the adherent rust. The final preparation grades were DSt2 according to standard ISO 8501-1: 2007.

2.1.3. Preparation of Rust Conversion Sample

Based on the phosphoric acid-gallic acid rust conversion system, a water-based RCC was prepared. Gallic acid was added to deionized water, magnetically stirred for 1 min, ultrasonicated for 3 min to make it completely dissolved, and then phosphoric acid of different mass fractions (2%, 3%, 5%) was added. The solution was stirred for 1 min to obtain component A. Texanol (film-forming assistants) was added to Haloflex 202 (film-forming substances) and stirred evenly for 15 min to obtain component B. Finally, A and Foamaster MO 2134AC (defoamer) were added to B, and stirred at low speed for 15 min. The composition is shown in Table 1.

Table 1. Coating formulation.

Material	Mass Concentration (%)
Gallic acid	0.2
Phosphoric acid	2–5
Haloflex 202	70
Texanol	2
Foamaster MO 2134AC	0.1
Distilled water	22.7–25.7

The rusted steel with adherent rust was rinsed with alcohol and dried. The water-based RCC was painted on the rusted steel surface. The rusted steel with RCC was dried for 6 h to ensure that the adherent rust was completely converted into a black conversion film (average thickness is <80 μm).

2.2. Analysis of Rust Conversion Performance

X-ray diffraction (XRD) used a Bruker D8 Advance (Bruker, Karlsruhe, Germany) with the monochromatic Cu Kα radiation, with a scanning rate of 4 °/min from 2θ = 10° up to 2θ = 80°. The XRD pattern was analyzed to determine the crystallographic information of the nonadherent rust, adherent rust and the effect of rust conversion.

The structure of the rust conversion products was further characterized by Fourier transform infrared (FTIR) to make up the deficiency of XRD. FTIR spectra data was collected by Thermo Nicolet iS10 (Thermo Fisher, Madison, WI, USA) with attenuated total reflection (ATR) technique. The wave numbers from 2000 to 525 cm^{-1} with the resolution 4 cm^{-1}.

The composition information of rusted steel before and after rust conversion was analyzed by Raman spectroscopy. The Raman spectra data was collected by Renishaw MZ20-FC (Renishaw, New Mills, UK) with the laser beam of He-Ne of 532 nm. The power of the laser was 1 mW to avoid the damage on the sample surface.

X-ray photoelectron spectroscopy (XPS) was used to analyze the change of element content and valence state on rusted steel surface before and after rust conversion. XPS data was collected by Thermo EscaLab 250Xi (Thermo Fisher, Madison, WI, USA) with Al Kα radiation (1486.6 eV), and the binding energy was calibrated using contaminant carbon at 284.8 eV.

2.3. Morphological and Compositional Characterization

Scanning electron microscopy (SEM, Hitachi Regulus8100, Hitachi, Tokyo, Japan) and energy dispersive spectrum (EDS, IXRF-SDD3330-A5501, TXRF, Austin, TX, USA) were used to observe the microscopic morphology and cross-sectional element distribution of the rusted steel before and after the RCC treatment. The laser scanning confocal microscopy (LSCM, Lext OLS5000, Olympus, Tokyo, Japan) was used to obtain the information of surface roughness of the sample. Before the cross-section observation, the sample (prepared in Section 2.1.3) was encapsulated in a PVC pipe with epoxy resin. After the epoxy resin was cured, the cross-section of the sample was polished step by step with waterproof abrasive paper to 2000#, and then rinsed with distilled water and dried.

2.4. Corrosion Resistance test

2.4.1. Electrochemical Measurements

The electrochemical measurements were performed in a coating evaluation electrolytic cell, using a Princeton P4000 electrochemical workstation (Ametek, Oak Ridge, TN, USA). The test area of the working electrode was controlled to be 1 cm^2 with the gasket of the electrolytic cell, and the test solution was 3.5 wt.% NaCl. Three-electrode system was adopted, the rusted steel before and after rust transformation was used as the working electrode, counter electrode was the platinum sheet, and the saturated calomel electrode (SCE) was connected to the Luggin-Haber capillary as the reference electrode. Faraday cage was used to shield external electromagnetic interference during the test. Before the

electrochemical measurement, the working electrode was immersed in the test solution and stabilized for at least 1 h until the open circuit potential (OCP) reaches a stable value (fluctuation within ±1 mV/min). The Tafel polarization curve was carried out in the range of ±250 mV relative to the open circuit potential (OCP), and the scanning speed was 1 mV/s.

2.4.2. Salt Spray Corrosion Resistance Test

According to ASTM B117-19 [26], a neutral salt spray test was used to evaluate the corrosion resistance of the rust conversion coating (RCC). The sample (30 × 60 × 2 mm^3) was rimmed with colophony and paraffin (mass ratio 1:1), and then was placed in salt spray chamber at an angle of 30°, sprayed for 12 h and stood for 12 h as a cycle. The corrosive medium was 5 ± 0.5 wt.% NaCl, the pH value was in the range of 6.5–7.2, and the temperature was 47 ± 0.5 °C. The protective performance and failure time of the rust conversion coating was obtained through the salt spray corrosion test.

2.4.3. Adhesion Experiment

The bonding strength between the coating and the steel substrate was tested according to the ISO 4624: 2002 standard [27] using a fully automatic drawing tester PosiTestAT-A produced by Delelsko, Ogdensburg, NY, USA. The bottom of the spindle was slightly abraded with 600# sandpaper and rinsed with alcohol. Araldite multifunctional adhesive (A:B = 1:1) was used to bond the surface of the RCC to the spindle (diameter 20 mm), and cured at room temperature for 24 h to ensure a good bonding effect. Circular cutter was used to cut a circle around the spindle to sperate the test area. Six pull-off tests were conducted on each type of samples, and the average value was the adhesion result.

3. Results and Discussion

3.1. Effect of PA on Rust Conversion and Solubility of GA

According to preliminary experiments, the dosage of Haloflex 202 (film-forming material), Texanol (film-forming assistant) and Foamaster MO 2134AC (defoamer) was determined. Considering the solubility limit of gallic acid [28] (S = 1.00 ± 0.02 g/100g water, 298.15 K), the dosage was determined to be 0.2 wt.%. The gallic acid and 2–5 wt.% phosphoric acid are applied to the water-based resin. The preparation process is shown in Section 2.1.3, and the formula refers to Table 1. After applying the water-based RCC, a black conversion film is formed on the surface of the rusted steel.

Figure 1(a1–a3) shows the appearance of the conversion film under different phosphoric acid additions. In the range of 2–5 wt.%, as the amount of phosphoric acid increases, the flatness of the conversion film decreases and blistering occurs. This is due to the excess phosphoric acid reacting with the steel matrix to produce gas. The best amount of phosphoric acid is 2 wt.%, the conversion film formed is the most smooth, dense and bright.

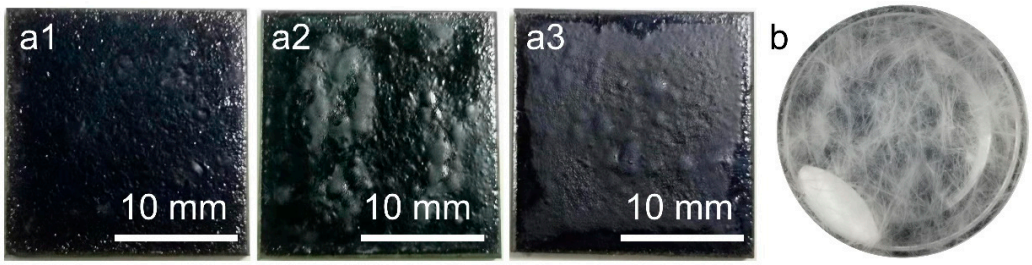

Figure 1. Effect of different amounts of PA on the rust conversion performance of GA: (**a1**) 2% PA, (**a2**) 3% PA, (**a3**) 5% PA, (**b**) flocculent precipitation.

In the process of preparing the coating, component A in Section 2.1.3 will gradually appear flocculent precipitation (Figure 1b) as the storage time increases. The precipitation may be gallic acid. Table 2 shows that based on the optimal ratio of component A

(Table 2(b5)), increasing the amount of phosphoric acid will result in faster precipitation. When the amount of phosphoric acid added is more than 5 g, the stability is less than 10 h. When the amount is 2 g, its stability is close to three days. Analyzing the conversion effect and the stability of component A, it is determined that the best formula is: gallic acid 0.2 wt.%, phosphoric acid 2 wt.%, Haloflex202 70 wt.%, Texanol 2 wt.%, Foamaster MO 2134AC 0.1 wt.%, and deionized water 25.7%. The RCC prepared below all adopt this formula.

Table 2. Flocculent precipitation schedule.

Sample	H_2O (mL)	GA (g)	PA (g)	Precipitation Time (h)
b1	25.7	0.2	10.0	1.0
b2	25.7	0.2	7.0	2.5
b3	25.7	0.2	5.0	10.0
b4	25.7	0.2	3.0	47.5
b5	25.7	0.2	2.0	70.5

3.2. Morphological and Compositional Characterization

3.2.1. Morphological and XRD Analysis

The pre-corroded Q235 steel is covered with a uniform rust layer, and the outer layer is nonadherent rust (Figure 2(a2)). Using a wire brush to remove nonadherent rust and then obtain a rusted steel with brown adherent rust (Figure 2(a1)). Figure 2(a4) shows that the use of component A in Section 2.1.3 on rusted steel will form insoluble blue-violet conversion products.

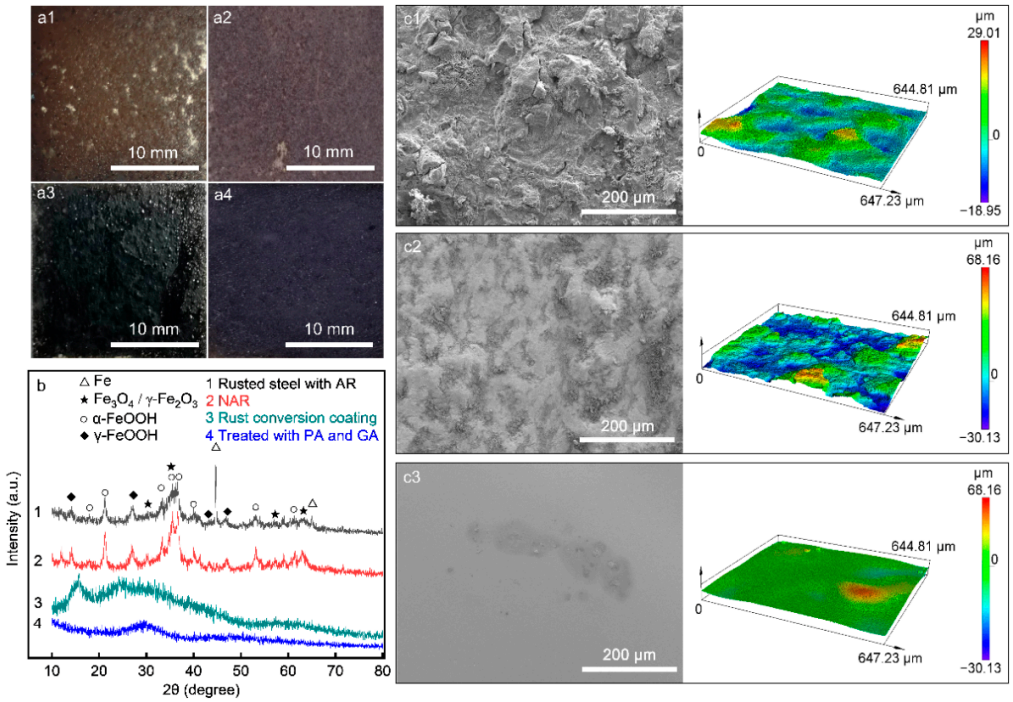

Figure 2. Optical images of (**a1**) Rusted steel with AR, (**a2**) NAR, (**a3**) Rust conversion coating and (**a4**) Treated with PA and GA. (**b**) XRD patterns of Rusted steel under different treatment states corresponding to (**a1**–**a4**). SEM and LSCM images of (**c1**) Rusted steel with AR, (**c2**) NAR and (**c3**) Rust conversion coating.

After applying the water-based RCC, the adherent rust reacts with phosphoric acid-gallic acid in the coating. The rust conversion products are fixed in the film-forming

substance and play a role in hindering the corrosive medium, and finally form a dense black film with corrosion resistance (Figure 2(a3)).

The nonadherent rust (NAR) is scraped off and collected, and then subjected to XRD testing. Figure 2b-2 shows that the main components of NAR are α-FeOOH and γ-FeOOH, and the spinel phase (Fe_3O_4 / γ-Fe_2O_3) is also detected. XRD cannot distinguish between Fe_3O_4 and γ-Fe_2O_3 with similar structures, so they are collectively referred to spinel phase [29,30]. The composition of the adherent rust (Figure 2b-1) is basically the same as the nonadherent rust, and a strong iron peak of the matrix is also detected. After the rust conversion treatment, the rust peak in the conversion coating (Figure 2b-3) and the conversion products (Figure 2b-4) disappeared. It shows that the rust had reacted with phosphoric acid-gallic acid. The conversion products exist in an amorphous form, which may be a mixture of phosphate and gallate [22,29].

Figure 2(c1–c3) are the SEM and LSCM images of the sample surface of Figure 2(a1–a3). The surface roughness parameters of different samples are listed in Table 3. After the nonadherent rust is removed, the grain profile of the rusted steel surface is more obvious. However, the surface roughness is reduced, and the arithmetic average height (Sa) is reduced from 11.77 μm to 4.55 μm. The arithmetic average height (Sa) of the sample coated with the rust conversion coating is 1.60 μm, which is smoother and denser than rusted steel. Careful observation revealed that there are still particles on the surface of the conversion film, which may be unreacted rust.

Table 3. Surface roughness parameters of different samples.

Sample	Sa (μm)	Sz (μm)	Sq (μm)	Sp (μm)	Sv (μm)
c1	4.55	45.33	5.89	25.58	19.74
c2	11.77	94.60	15.20	57.44	37.16
c3	1.60	23.44	2.14	9.55	13.88

3.2.2. FTIR analysis

The component A in Section 2.1.3 is applied to the surface of adherent rust to obtain the rust conversion products. XRD analysis shows that the components of nonadherent rust and adherent rust were consistent, so the FTIR was carried out using nonadherent rust instead of rusted steel. Figure 3a shows that the nonadherent rust has characteristic absorption peaks of γ-FeOOH at 1020, 1462 and 1632 cm^{-1}, α-FeOOH at 797 and 879 cm^{-1}, and Fe_3O_4 at 568 cm^{-1} [13,22,24]. The results of FTIR spectra analysis of rust products are consistent with XRD. Other studies also believe that α-FeOOH, γ-FeOOH and Fe_3O_4 are the compounds most commonly found in atmospheric corrosion [19].

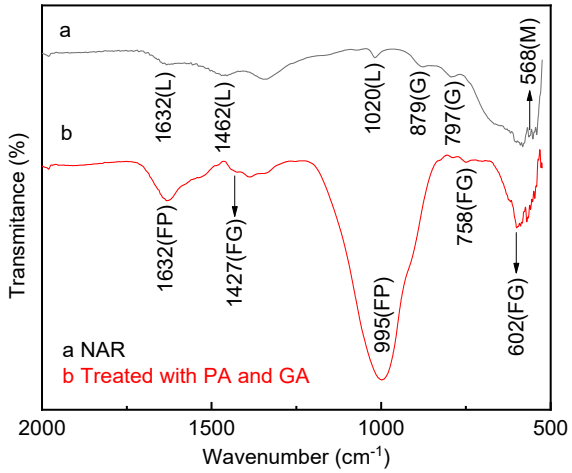

Figure 3. FTIR spectra of (**a**) NAR, (**b**) Treated with PA and GA (L: lepidocrocite, G: goethite, M: magnetite, FP: ferric phosphate, FG: ferric gallate).

Figure 3b shows that the conversion products formed a broad peak at 995 cm^{-1} and a peak at 1632 cm^{-1} to characterize the presence of ferric phosphate [31]. The absorption peaks at 602, 758 and 1427 cm^{-1} indicate the presence of blue-violet ferric gallate in the conversion products [22]. The above analysis shows that the phosphoric acid-gallic acid rust conversion system can react with adherent rust to form a mixture of ferric phosphate and ferric gallate.

3.3. Properties of Rust Conversion Coating

3.3.1. Tafel Curve Analysis

The Tafel curve was performed on the Q235 steel, the rusted steel with adherent rust (AR) and the rust conversion coating, and the results are shown in Figure 4. The fitting results of the Tafel curve are listed in Table 4. The corrosion potential (E_{corr}) of rusted steel (−0.632 V) is more positive than Q235 steel (−0.677 V), indicating that its corrosion tendency becomes lower. However, the corrosion current density (I_{corr}) of rusted steel (2.320×10^{-4} A/cm^2) is greater than Q235 steel (7.051×10^{-6} A/cm^2). It may be that the adherent rust on the steel surface has no protective effect, but instead promotes the corrosion. The sample treated with the rust conversion coating has the lowest corrosion current density (1.902×10^{-7} A/cm^2), which is three orders of magnitude lower than that of the rusted steel. The corrosion potential of rusted steel coated with RCC (−0.606 V) is more positive than Q235 steel and rusted steel with AR. It means that rusted steel coated with RCC has the lowest corrosion tendency. According to the Tafel polarization slope, the corrosion reaction of Q235 steel is controlled by cathodic polarization ($-\beta_c = 0.293$). The corrosion reaction of rusted steel with AR is controlled by anodic polarization ($\beta_a = 0.252$). The anodic/cathodic polarization slopes of the rust conversion coating were 0.220 and 0.217, respectively. It shows that the rust conversion coating retards both the cathodic and anodic reaction processes of the corrosion. The Tafel curve analysis proved the good corrosion resistance of rust conversion coating.

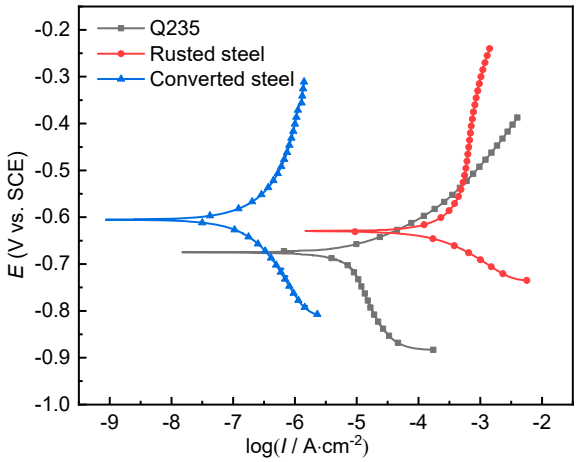

Figure 4. Tafel polarization curves of samples before and after rust conversion treatment.

Table 4. Corrosion parameters calculated from Tafel polarization curves measured in Figure 4.

Samples	E_{corr} (V vs. SCE)	β_a (V/dec)	$-\beta_c$ (V/dec)	I_{corr} (A/cm^2)
Q235	−0.677	0.061	0.293	7.051×10^{-6}
Rusted Steel with AR	−0.632	0.252	0.087	2.320×10^{-4}
Rust Conversion Coating	−0.606	0.220	0.217	1.902×10^{-7}

3.3.2. Salt Spray Test

Figure 5 shows the salt spray corrosion resistance of the steel plates before and after applying the RCC. Both bare steel and rusted steel with AR undergo severe corrosion in a

short period. Rusted steel with AR corrodes faster than bare steel, and bare steel has some uncorroded areas on the 7th day. The rusted steel with AR treated by the rust conversion coating forms a black rust conversion film. In the early stage of the salt spray test, the rust conversion film has no blistering, cracking and corrosion. The conversion coating did not appear pitting until the 20th day (Figure 5(c3)). The salt spray test shows that the rust conversion coating can effectively prevent the entry of corrosive media and has good corrosion resistance.

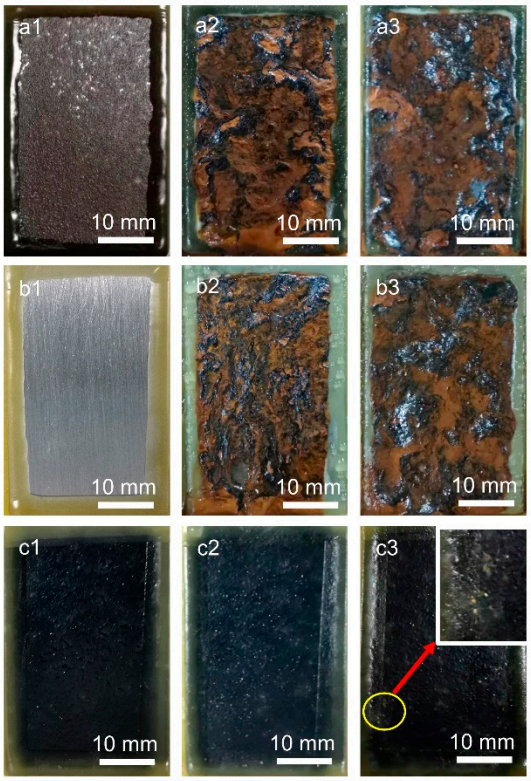

Figure 5. The surface state of the steel plates before and after rust conversion treatment under salt spray test on 1d (**a1**,**b1**,**c1**)—7d (**a2**,**b2**,**c2**)—20d (**a3**,**b3**,**c3**): (**a1**–**a3**) Rusted steel with AR, (**b1**–**b3**) Bare steel, (**c1**–**c3**) RCC.

3.3.3. Adhesion Test

Using epoxy adhesive (Araldite multifunctional adhesive) to bond spindle and steel substrate. After the adhesion test is completed, the spindle will be separated from the substrate, showing the interface morphology shown in Figure 6. In the adhesion test, there will be three possible failure forms, including (1) interfacial fracture, (2) cohesive fracture, and (3) mixed fracture. Analyzing the failure form of adhesion test will help to understand the failure mechanism and further improve the adhesion [32,33].

Figures 6 and 7 reflect the interface morphology and adhesion strength of different samples. As shown in Figure 6a, the failure form between the epoxy adhesive and the rusted steel is the cohesive failure of adherent rust. The adhesion strength of the adherent rust is 1.85 MPa, which affects the adhesion of the coating system. Figure 6b shows that after the rust conversion treatment, the phosphoric acid-gallic acid in the coating reacted with the adherent rust to form a black conversion film. The original adherent rust changed from brown to dark gray, and there were some black aggregate particles. Therefore, the surface of the rusted steel after treatment may include rust conversion products and unreacted rust, which is in line with the typical structure of conversion film [34]. The adhesion strength of the sample increased from 1.85 MPa to 2.75 MPa. The rust conversion coating has good adhesion, but the unreacted rust is still the key to limiting the improvement of adhesion. Figure 6c shows that after the rust conversion coating is applied to bare steel, the interface

failure occurs between the substrate and the rust conversion coating. On the surface of bare steel without rust, phosphoric acid-gallic acid can still react with the iron matrix to form a conversion film. The result shows that the ideal adhesion strength of the conversion coating is 7.44 MPa without being affected by unreacted rust.

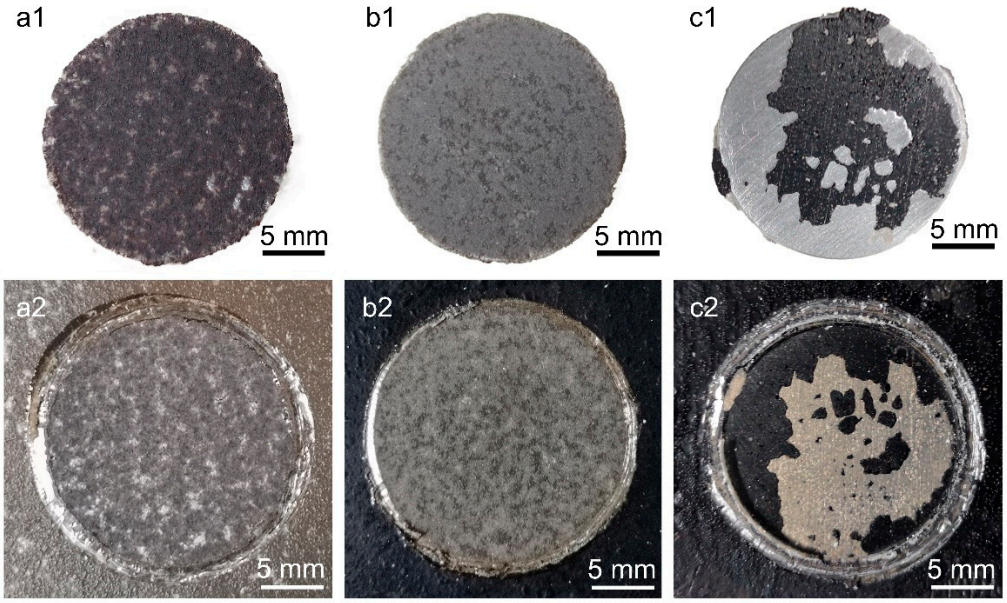

Figure 6. Fracture surface morphologies of (**a**) RS, (**b**) RS coated with RCC, (**c**) BS coated with RCC: (1) spindle, (2) substrate (RS: rusted steel, BS: bare steel, RCC: rust conversion coating).

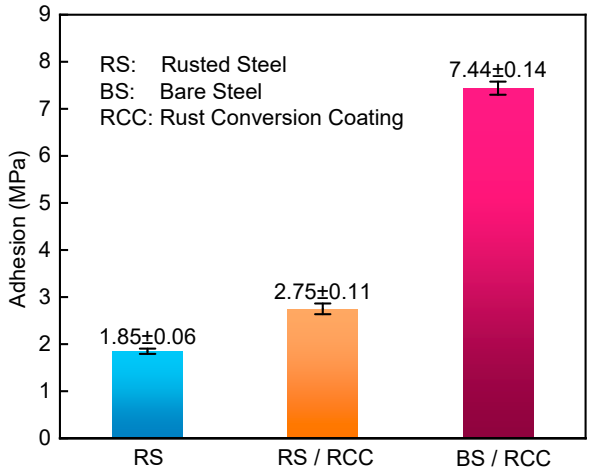

Figure 7. Adhesion strength of different samples corresponding to Figure 6.

3.4. Structure and Mechanism of Rust Conversion Coating

3.4.1. Raman Spectroscopy

Raman spectroscopy was used to analyze the surface composition of the rusted steel with AR (Figure 6(a2)) and the rust conversion substrate (Figure 6(b2)). As shown in Figure 8, the Raman peaks of rusted steel with AR (Figure 8a) correspond to γ-FeOOH (216 and 1307 cm^{-1}), α-FeOOH (245 and 394 cm^{-1}) and Fe_3O_4 (669 cm^{-1}) [35–38]. Compared with the rusted steel with AR, the peak at 245 cm^{-1} disappeared in the rust conversion substrate (Figure 8b). The other peaks did not change significantly. The results indicate that there is still unreacted rust. The 1004 cm^{-1} peak representing ferric phosphate appeared [39]. It shows that ferric phosphate not only appeared in the conversion coating,

but also attached to the surface of the rust conversion substrate. This is further confirmed in Figure 10c.

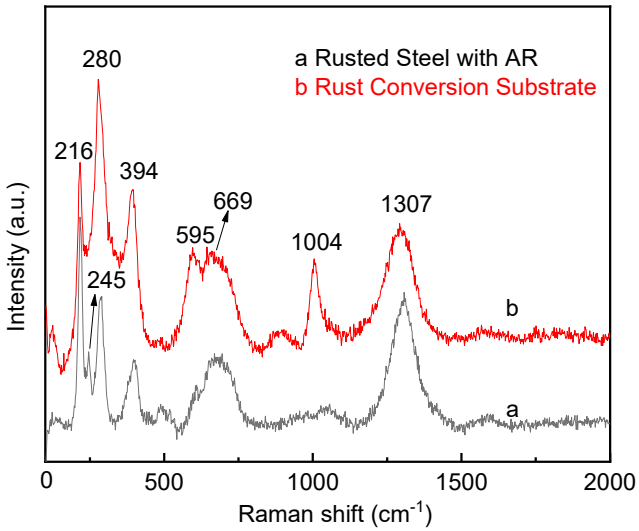

Figure 8. Raman spectra of (**a**) Rusted Steel with AR and (**b**) Rust Conversion Substrate.

3.4.2. XPS Analysis

The XPS technology was used to analyze the rusted steel with AR and the rust conversion substrate, as shown in Figure 9. The P2p peak appears on the surface of the rust conversion substrate, indicating the presence of phosphate. This is consistent with the Raman and EDS analysis in Section 3.4.3. Cl2p and Na KL1 peaks appear in the spectrum, which may be NaCl introduced in the pre-corrosion process of the steel plate. Figure 9 and Table 5 show that the binding energy of the O1s peak increased from 529.87 eV to 531.18 eV after the rust conversion treatment of rusted steel. This may be due to the formation of C–O–Fe bonds by the reaction of gallic acid and rust. Carbon has a strong electronegativity, which reduces the electron density of oxygen atoms and increases the binding energy of oxygen atoms. The ferrous complex produced by the reaction of gallic acid and rust will eventually be oxidized to ferric complex in the air [22,23].

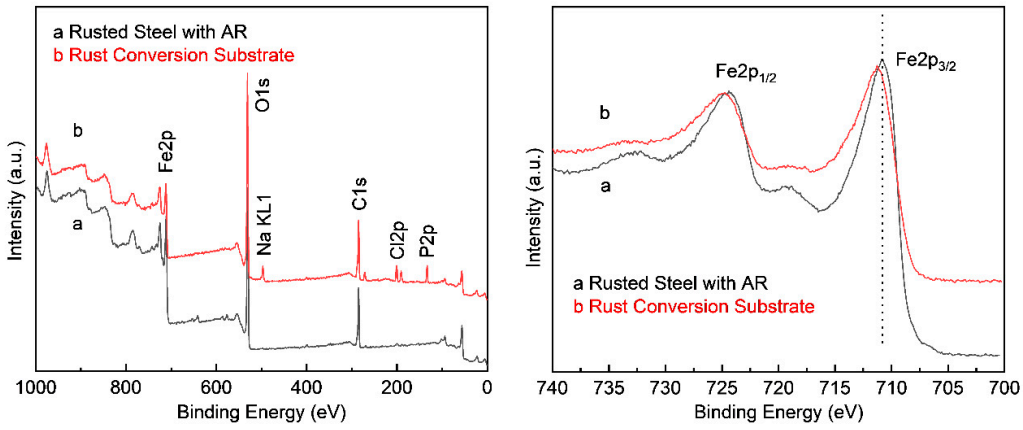

Figure 9. XPS spectrum and specific element peaks of (**a**) Rusted Steel with AR and (**b**) Rust Conversion Substrate.

Table 5. Binding energies of various elements in (**a**) Rusted Steel with AR and (**b**) Rust conversion Substrate.

Element	Sample	Binding Energy (eV)
Fe2p	a	710.77 ($Fe2p_{3/2}$), 724.38 ($Fe2p_{1/2}$)
	b	711.28 ($Fe2p_{3/2}$), 724.78 ($Fe2p_{1/2}$)
O1s	a	529.87
	b	531.18

3.4.3. Element Distribution and Mechanism Analysis

Figure 10a,b shows the cross-sectional morphology of the rusted steel before and after the rust conversion treatment and the corresponding element scans of the rust conversion film. The cross section of the rusted steel has a porous structure, and the thickness of the rust layer is in the range of 30–70 µm. After using the RCC, the rust is significantly reduced. Adherent rust reacts with the rust converters to form a compact conversion film (RCF, thickness 70–80 µm). The cross-section includes a three-layer structure: rust conversion film, unreacted rust and Q235 steel. The cross-sectional morphology further confirms the analysis of unreacted rust after rust conversion treatment in Sections 3.2.1 and 3.4.1.

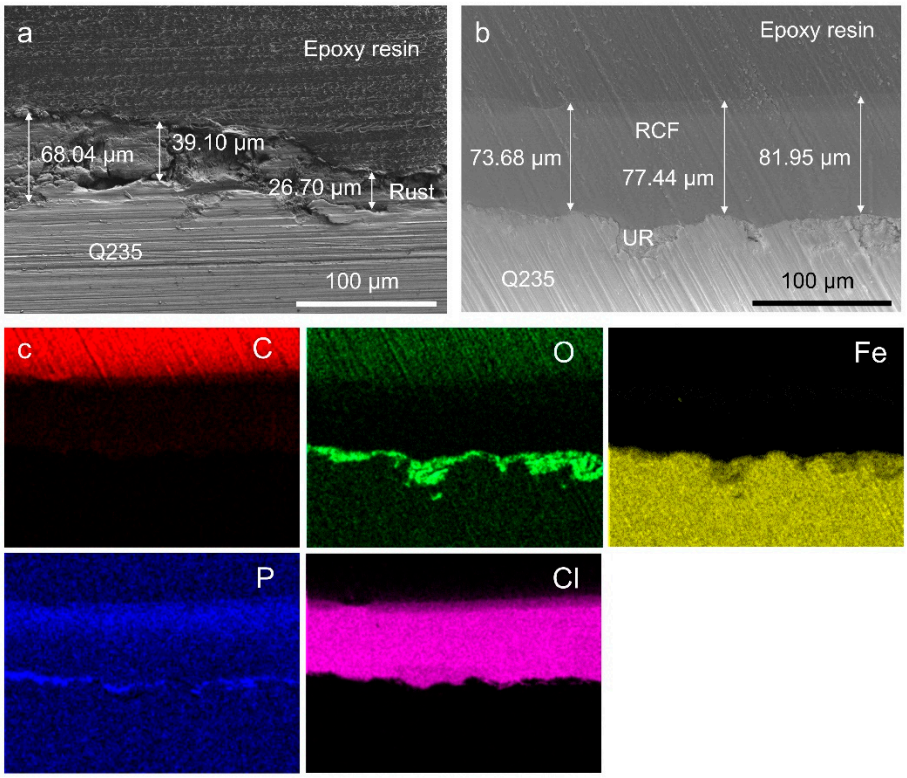

Figure 10. Cross-section micrographs of rusted steel before (**a**) and after (**b**) rust conversion treatment and the chemical mapping (**c**) of C, O, Fe, P, Cl belonging to (**b**) (RCF: Rust conversion film, UR: Unreacted Rust).

The element scan (Figure 10c) of the cross-section shows that the RCF contains C, P and Cl elements. Haloflex 202 is a vinyl chloride acrylic emulsion, which contains a large amount of Cl element. This confirms that the conversion film consists of ferric phosphate, ferric gallate, and Haloflex 202. The distribution of P element (Figure 10c) shows that phosphoric acid is more likely to react with rust and enter the inside of adherent rust. Eventually, the formed ferric phosphate accumulates in the RCF and on the surface of unreacted rust.

According to the cross-sectional SEM and EDS of the RCC system in Figure 10b,c, the rust conversion mechanism of phosphoric acid-gallic acid in vinyl chloride acrylic emulsion is proposed, as shown in Figure 11. XRD and FTIR analysis show that the amorphous conversion products were a mixture of ferric gallate and ferric phosphate. Conversion products and vinyl chloride acrylic emulsion together form RCF. Raman spectroscopy shows that rust does not completely react with the rust converter, and there is still unreacted rust. Figure 2(c3), Figure 6(b2) and Figure 10c also confirm this view. Part of the rust will dissolve into Fe^{2+} and Fe^{3+} at the interface between the rust conversion coating and the unreacted rust, and further generate conversion products. Phosphoric acid reacts fastest with γ-FeOOH, followed by Fe_3O_4 and α-FeOOH [13]. The EDS (Figure 10c) shows that the formed ferric phosphate accumulates in the RCF and on the surface of unreacted rust. Gallic acid has reducing properties and will reduceFe^{3+} to ferrous complexes. Under the action of oxygen, the ferrous complex will be oxidized into insoluble ferric complex [22]. This can be confirmed in the XPS analysis. Therefore, the reaction of phosphoric acid-gallic acid in this study is as Equations (1)–(3):

$$Fe^{3+} + PO_4^{3-} \rightarrow FePO_4 \quad (1)$$

$$Fe^{3+} + 2\{R(OH)_{n-1}O^-\} + e^- \rightarrow Fe\{R(OH)_{n-1}O\}_2 \quad (2)$$

$$2Fe\{R(OH)_{n-1}O\}_2 + 2R(OH)_{n-1}O^- + 1/2O_2 + 2H^+ = 2Fe\{R(OH)_{n-1}O\}_3 + H_2O \quad (3)$$

Finally, RCF containing insoluble conversion products covers the steel. It can prevent the corrosive medium from contacting the steel. The residual phosphoric acid and gallic acid in the conversion film can also continue to react with the dissolved iron ions, thereby preventing the corrosion reaction from proceeding.

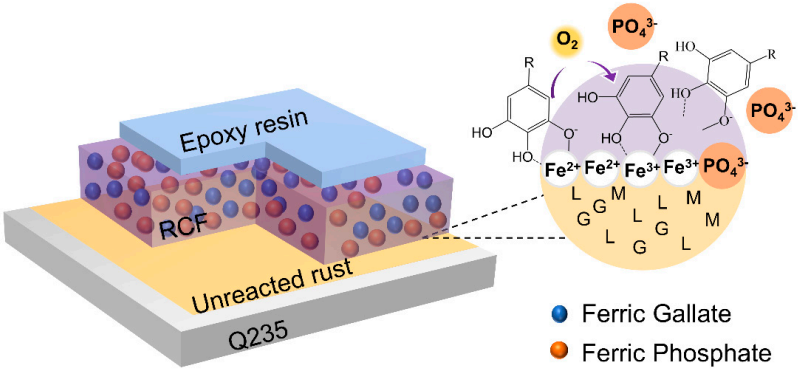

Figure 11. Proposed scheme for the rust conversion mechanism of phosphate acid-gallic acid in vinyl chloride acrylic emulsion (RCF: rust conversion film, L: lepidocrocite, G: goethite, M: magnetite).

4. Conclusions

This work studies the rust conversion performance of phosphoric acid-gallic acid in vinyl chloride acrylic emulsion. From the results obtained, the following conclusions can be drawn:

1. The phosphoric acid-gallic acid conversion system with reasonable film-forming substances, film-forming assistants and defoamers can be used in vinyl chloride acrylic emulsions. When the dosage of gallic acid is 0.2 wt.%, Haloflex 202 is 70 wt.%, Texanol is 2 wt.%, Foamaster MO 2134AC is 0.1 wt.%, and phosphoric acid is 2 wt.%, the best synergistic conversion effect is achieved.
2. The rust conversion coating can effectively treat the rusted steel produced by simulating marine atmospheric corrosion. The conversion products ferric phosphate and ferric gallate can form a black conversion film with vinyl chloride acrylic emulsion. It can retard both the cathodic and anodic reaction processes of the corrosion. After rust

conversion treatment, the corrosion current density is reduced to 1.902×10^{-7} A/cm^2, and the salt spray corrosion resistance reaches 20d.

3. After the rust conversion treatment, the adhesion strength of the coating system increased to 2.75 MPa. The unreacted rust between the Q235 substrate and the rust conversion film affects the further improvement of adhesion. Unreacted rust is still the limiting link to improve the anti-corrosion performance of rust conversion coatings.

Author Contributions: Conceptualization, B.H., Q.Z. and X.W.; methodology, X.W. and Q.Z.; formal analysis, X.W. and X.L.; investigation, X.W. and Q.Z.; resources, B.H. and Q.Z.; writing, X.W. and Q.Z.; supervision, B.H. and Q.Z. All authors read and agreed to the published version of the manuscript.

Funding: This work was financially supported by the National Natural Science Foundation of China (Grant No. 41827805) and Shandong Provincial Natural Science Foundation (No. ZR2020MD080).

Institutional Review Board Statement: Not applicable.

Informed Consent Statement: Not applicable.

Data Availability Statement: The data presented in this study are available in article.

Conflicts of Interest: The authors declare no conflict of interest.

References

1. Bhaskaran, R.; Bhalla, L.; Rahman, A.; Juneja, S.; Sonik, U.; Kaur, S.; Kaur, J.; Rengaswamy, N.S. An analysis of the updated cost of corrosion in India. *Mater. Perform.* **2014**, *53*, 56–65.
2. Hou, B.; Li, X.; Ma, X.; Du, C.; Zhang, D.; Zheng, M.; Xu, W.; Lu, D.; Ma, F. The cost of corrosion in China. *Npj Mater. Degrad.* **2017**, *1*, 1–10. [CrossRef]
3. Kodama, T. Corrosion cost survey in Japan—Focusing on transportation industry. *Corros. Sci. Tech.* **2008**, *7*, 252–258.
4. Sik, K.Y.; Lim, H.K.; Kim, J.J.; Suk, H.W.; Soo, P.Y. Corrosion cost and corrosion map of Korea - Based on the data from 2005 to 2010. *Corros. Sci. Tech.* **2011**, *10*, 52–59.
5. Thompson, N.G.; Yunovich, M.; Dunmire, D. Cost of corrosion and corrosion maintenance strategies. *Corros. Rev.* **2007**, *25*, 247–261. [CrossRef]
6. *ISO 8501-1: 2007 Preparation of Steel Substrates before Application of Paints and Related Products—Visual Assessment of Surface Cleanliness—Part 1: Rust Grades and Preparation Grades of Uncoated Steel Substrates and of Steel Substrates after Overall Removal of Previous Coatings*; ISO: Geneva, Switzerland, 2007.
7. Alcantara, J.; Chico, B.; Simancas, J.; Diaz, I.; de la Fuente, D.; Morcillo, M. An attempt to classify the morphologies presented by different rust phases formed during the exposure of carbon steel to marine atmospheres. *Mater. Charact.* **2016**, *118*, 65–78. [CrossRef]
8. Morris, R.V.; Lauer, H.V.; Lawson, C.A.; Gibson, E.K.; Nace, G.A.; Stewart, C. Spectral and other physicochemical properties of submicron powders of hematite (alpha-Fe_2O_3), Maghemite (gamma-Fe_2O_3), Magnetite (Fe_3O_4), Goethite (alpha-FeOOH), and Lepidocrocite (gamma-FeOOH). *J. Geophys. Res.* **1985**, *90*, 3126–3144. [CrossRef]
9. Murkute, P.; Kumar, R.; Choudhary, S.; Maharana, H.S.; Ramkumar, J.; Mondal, K. Comparative atmospheric corrosion behavior of a mild steel and an interstitial free steel. *J. Mater. Eng. Perform.* **2018**, *27*, 4497–4506. [CrossRef]
10. Raman, A.; Nasrazadani, S.; Sharma, L. Morphology of rust phases formed on weathering steels in various laboratory corrosion tests. *Metallography* **1989**, *22*, 79–96. [CrossRef]
11. Barrero, C.A.; Garcia, K.E.; Morales, A.L.; Greneche, J.M. A proposal to evaluate the amount of corroded iron converted into adherent rust in steels exposed to corrosion. *Corros. Sci.* **2011**, *53*, 769–775. [CrossRef]
12. Saji, V.S. Progress in rust converters. *Prog. Org. Coat.* **2019**, *127*, 88–99. [CrossRef]
13. Nasrazadani, S. The application of infrared spectroscopy to a study of phosphoric and tannic acids interactions with magnetite (Fe3O4), goethite (alpha-FeOOH) and lepidocrocite (gamma-FeOOH). *Corros. Sci.* **1997**, *39*, 1845–1859. [CrossRef]
14. Xu, W.; Han, E.-H.; Wang, Z. Effect of tannic acid on corrosion behavior of carbon steel in NaCl solution. *J. Mater. Sci. Technol.* **2019**, *35*, 64–75. [CrossRef]
15. Cerisola, G.; Barbucci, A.; Caretta, M. Organic coatings for marginally prepared steel surfaces. *Prog. Org. Coat.* **1994**, *24*, 21–28. [CrossRef]
16. Gust, J.; Suwalski, J. Use of mossbauer-spectroscopy to study reaction-products of polyphenols and iron compounds. *Corrosion* **1994**, *50*, 355–365. [CrossRef]
17. Matamala, G.; Smeltzer, W.; Droguett, G. Comparison of steel anticorrosive protection formulated with natural tannins extracted from acacia and from pine bark. *Corros. Sci.* **2000**, *42*, 1351–1362. [CrossRef]
18. Gust, J.; Bobrowicz, J. Sealing and anti-corrosive action of tannin rust converters. *Corrosion* **1993**, *49*, 24–30. [CrossRef]
19. Gust, J. Application of infrared-spectroscopy for investigation of rust phase component conversion by agents containing oak tannin and phosphoric-acid. *Corrosion* **1991**, *47*, 453–457.

20. Collazo, A.; Novoa, X.R.; Perez, C.; Puga, B. The corrosion protection mechanism of rust converters: An electrochemical impedance spectroscopy study. *Electrochim. Acta* **2010**, *55*, 6156–6162. [CrossRef]
21. Zhao, X.D.; Cheng, Y.F.; Fan, W.; Vladimir, C.; Volha, V.; Alla, T. Inhibitive performance of a rust converter on corrosion of mild steel. *J. Mater. Eng. Perform.* **2014**, *23*, 4102–4108. [CrossRef]
22. Favre, M.; Landolt, D. The influence of gallic acid on the reduction of rust on painted steel surfaces. *Corros. Sci.* **1993**, *34*, 1481–1494.
23. Jia, Y.; Ren, N.; Yue, H.; Deng, J.; Liu, Y. Preparation and properties of natural gallic acid based rust conversion emulsion. *Pigm. Resin Technol.* **2016**, *45*, 191–198. [CrossRef]
24. Feng, L.; Yuan, P. Corrosion protection mechanism of aluminum triphosphate modified by organic acids as a rust converter. *Prog. Org. Coat.* **2020**, *140*, 105508. [CrossRef]
25. Diaz, B.; Figueroa, R.; Novoa, X.R.; Perez, C.; Pintos, A. The corrosion protection afforded by a commercial rust converter doped with graphene oxide. *Electrochim. Acta* **2020**, *342*, 136096. [CrossRef]
26. *ASTM B117-19 Standard Practice for Operating Salt Spray (Fog) Apparatus*; ASTM: West Conshohocken, PA, USA, 2019; Volume 03.02.
27. *ISO 4624: 2002 Paints and Varnishes—Pull-Off Test for Adhesion*; ISO: Geneva, Switzerland, 2007.
28. Lu, L.-L.; Lu, X.-Y. Solubilities of gallic acid and its esters in water. *J. Chem. Eng. Data* **2007**, *52*, 37–39. [CrossRef]
29. Collazo, A.; Novoa, X.R.; Perez, C.; Puga, B. EIS study of the rust converter effectiveness under different conditions. *Electrochim. Acta* **2008**, *53*, 7565–7574. [CrossRef]
30. Alcantara, J.; Chico, B.; Diaz, I.; de la Fuente, D.; Morcillo, M. Airborne chloride deposit and its effect on marine atmospheric corrosion of mild steel. *Corros. Sci.* **2015**, *97*, 74–88. [CrossRef]
31. Ocampo, L.M.; Margarit, I.C.P.; Mattos, O.R.; Cordoba-De-Torresi, S.I.; Fragata, F.L. Performance of rust converter based in phosphoric and tannic acids. *Corros. Sci.* **2004**, *46*, 1515–1525.
32. Li, Y.; Ma, Y.; Zhang, B.; Lei, B.; Li, Y. Enhancement the adhesion between epoxy coating and rusted structural steel by tannic acid treatment. *Acta Met. Sin-Engl.* **2014**, *27*, 1105–1113. [CrossRef]
33. Tang, F.; Sao, Y.; Chen, Y.; Tang, Y.; Chen, G. Impact and corrosion resistances of duplex epoxy/enamel coated plates. *Constr. Build. Mater.* **2016**, *112*, 7–18. [CrossRef]
34. Ross, T.K.; Francis, R.A. Treatment of rusted steel with mimosa tannin. *Corros. Sci.* **1978**, *18*, 351–361. [CrossRef]
35. De la Fuente, D.; Alcantara, J.; Chico, B.; Diaz, I.; Jimenez, J.A.; Morcillo, M. Characterisation of rust surfaces formed on mild steel exposed to marine atmospheres using XRD and SEM/Micro-Raman techniques. *Corros. Sci.* **2016**, *110*, 253–264. [CrossRef]
36. Morcillo, M.; Chico, B.; Alcantara, J.; Diaz, I.; Wolthuis, R.; de la Fuente, D. SEM/Micro-raman characterization of the morphologies of marine atmospheric corrosion products formed on mild steel. *J. Electrochem. Soc.* **2016**, *163*, C426–C439. [CrossRef]
37. Morcillo, M.; Wolthuis, R.; Alcantara, J.; Chico, B.; Diaz, I.; de la Fuente, D. Scanning Electron Microscopy/Micro-Raman: A very useful technique for characterizing the morphologies of rust phases formed on carbon steel in atmospheric exposures. *Corrosion* **2016**, *72*, 1044–1054.
38. Yang, J.; Lu, Y.; Guo, Z.; Gu, J.; Gu, C. Corrosion behaviour of a quenched and partitioned medium carbon steel in 3.5 wt.% NaCl solution. *Corros. Sci.* **2018**, *130*, 64–75. [CrossRef]
39. Gu, Z.; Liao, Y.; Zhang, Z.; Guo, Q.; Su, F. Raman spectroscopic study on mechanism of aluminum triphosphate pigment. *Electrochemistry* **2002**, *8*, 32–39.